JGR Space Physics

RESEARCH ARTICLE
10.1029/2019JA027546

Key Points:
- First imaging measurement of the electron-impact N_2 LBH cascade-induced spectrum at energies of 30–200 eV is presented
- Cascading transition to the N_2 a-state (a' and $w \rightarrow a$) from radiative and collision-induced-electronic transitions (CIETs)
- We present LBH band intensities at various pressures and electron impact direct and cascade LBH emission cross sections from 40–200 eV

Supporting Information:
- Supporting Information S1

Correspondence to:
J. M. Ajello,
joe.ajello@lasp.colorado.edu

Citation:
Ajello, J. M., Evans, J. S., Veibell, V., Malone, C. P., Holsclaw, G. M., Hoskins, A. C., et al. (2020). The UV spectrum of the Lyman-Birge-Hopfield band system of N_2 induced by cascading from electron impact. *Journal of Geophysical Research: Space Physics*, *125*, e2019JA027546. https://doi.org/10.1029/2019JA027546

Received 12 NOV 2019
Accepted 29 JAN 2020
Accepted article online 6 FEB 2020

The UV Spectrum of the Lyman-Birge-Hopfield Band System of N_2 Induced by Cascading from Electron Impact

Joseph M. Ajello[1], J. Scott Evans[2], Victoir Veibell[2], Charles P. Malone[3], Greg M. Holsclaw[1], Alan C. Hoskins[1], Rena A. Lee[1,4], William E. McClintock[1], Saurav Aryal[1], Richard W. Eastes[1], and Nicholas Schneider[1]

[1]Laboratory for Atmospheric and Space Physics, University of Colorado, Boulder, CO, [2]Computational Physics Inc., Springfield, VA, [3]Jet Propulsion Laboratory, California Institute of Technology, Pasadena, CA, [4]Department of Physics & Astronomy, Vassar College, Poughkeepsie, NY

Abstract We have measured in the laboratory the far ultraviolet (FUV: 125.0–170.0 nm) cascade-induced spectrum of the Lyman-Birge-Hopfield (LBH) band system ($a^1\Pi_g \rightarrow X^1\Sigma_g^+$) of N_2 excited by 30–200 eV electrons. The cascading transition begins with two processes: radiative and collision-induced electronic transitions (CIETs) involving two states ($a'^1\Sigma_u^-$ and $w^1\Delta_u \rightarrow a^1\Pi_g$), which are followed by a cascade induced transition $a^1\Pi_g \rightarrow X^1\Sigma_g^+$ at the single-scattering pressures employed here. Direct excitation to the a-state produces a confined LBH spectral glow pattern around an electron beam. We have spatially resolved the electron-induced glow pattern from an electron beam colliding with N_2 at radial distances of 0–400 mm at three gas pressures. This imaging measurement is the first to isolate spectral measurements in the laboratory of single-scattering electron-impact-induced fluorescence from two LBH emission processes: direct excitation, which is strongest in emission near the electron beam axis; and cascading-induced, which is dominant far from the electron beam axis. The vibrational populations for vibrational levels from v′ = 0–2 of the $a\ ^1\Pi_g$ state are enhanced by radiative cascade and CIETs, and the emission cross sections of the LBH band system for direct and cascading-induced excitation are provided at 40, 50, 100, and 200 eV.

1. Introduction

The study of the Lyman-Birge-Hopfield (LBH) band system ($a^1\Pi_g \rightarrow X^1\Sigma_g^+$) of N_2 in the laboratory by UV spectroscopy has heretofore failed to measure the cascade-induced UV spectrum and determine LBH vibrational intensities or cascade emission cross sections. This failure has precipitated a controversy in the literature that has persisted for over a decade due to the dichotomy between terrestrial airglow observations and model calculations (Budzien et al., 1994; Cartwright, 1978; Eastes, 2000; Eastes & Dentamaro, 1996). Analysis of terrestrial far ultraviolet (FUV) airglow spectra is aimed at determining the abundances of the major constituents of the upper thermosphere: N_2, O_2, and O. The retrieval of thermospheric column abundance ratio O/N_2 (also referred to as $\Sigma\ O/N_2$ in the literature) depends upon N_2 LBH and O emission cross sections (Evans et al., 1995; Strickland et al., 1995, 1999). The relative vibrational distributions of the LBH band system observed in the dayglow and aurora sometimes agree with theoretical calculations for direct impact (Ajello, 1970; Ajello & Shemansky, 1985), and other times statistically significant departures of 30–50% occur (Ajello et al., 2011; Budzien et al., 1994; Eastes & Dentamaro, 1996). We can thus shed light on the origin of the difference in the UV spectrum between laboratory and space-borne measurements. The principal cause is the pressure-dependent lifetimes and energy-dependent cross sections for cascade to the a-state from the ($a'^1\Sigma_u^-$ and $w^1\Delta_u \rightarrow a^1\Pi_g \rightarrow X^1\Sigma_g^+$) states by two separate processes: radiative cascade *and* collision-induced-electronic transitions (CIETs).

The $a\ ^1\Pi_g$ state is itself metastable from direct excitation being magnetic dipole and electric quadrupole in character. Only single collisions occur in this experiment since N_2 molecules directly excited to the a-state travel up to 10 cm (to the 99.7% 3σ-level) before radiating (Ajello et al., 2017; Marinelli et al., 1989). The lifetimes of the cascade states are markedly longer, requiring a large vacuum system to observe and fully measure both forbidden radiation sources beyond this 10 cm limit. Our imaging experiment is the first to measure and isolate the optical emissions of single-scattering (i.e., low-pressure) electron-impact-induced-

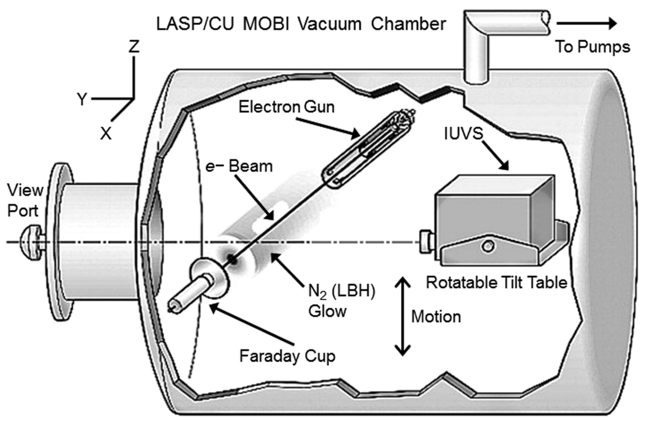

Figure 1. Experimental schematic of N_2 LBH glow experiment composed of a 0.3 m electrostatic electron gun and MAVEN IUVS mounted to a positioning table housed in MOBI. Reproduced from Ajello et al. (2017).

fluorescence from both direct excitation of the $a\ ^1\Pi_g$ state and cascade-induced-fluorescence contributions to the $a\ ^1\Pi_g$ state. There is marked difference between the a'-state and w-state lifetimes to the ground state. The a'-state lifetime is found to be ~40 ms by Wilkinson (1959), while Tilford and Benesch (1976) find the lifetime to be ~13 ms for $v' = 0$, noting that $a'(0)$ energetically resides below $a(0)$. More recently, Eastes and Dentamaro (1996) recommend a lifetime of ~17 ms for the $a'\,^1\Sigma_u^- \rightarrow X^1\Sigma_g^+$ forbidden transition (that proceeds through nearby $^1\Pi_u$ states). The w-state is dipole forbidden from the ground state and can only be depopulated by CIET or radiative cascade decay to the a-state with a radiative lifetime to the ground state on the order of seconds for the forbidden $w^1\Delta_u \rightarrow X^1\Sigma_g^+$ transition. In this paper, we discuss the dipole-allowed transitions ($a'^1\Sigma_u^-$ and $w\ ^1\Delta_u \rightarrow a\ ^1\Pi_g$) in section 3. We also present measurement results of LBH vibrational band intensities from 30–200 eV at different pressures and provide electron impact cross sections for cascade and direct excitation of LBH at 40–200 eV energy range.

2. Experimental Apparatus

In the past we have constructed a large (1.5 m-diameter) vacuum system apparatus for measuring the emission cross sections of the strongest optically forbidden transitions found in solar system planetary atmosphere airglow: N_2 LBH (Ajello et al., 2017), O I 135.6 nm from O_2 (Kanik et al., 2003; Noren et al., 2001), and O I 135.6 nm from CO and CO_2 (Ajello et al., 2019), as well as the Cameron bands from CO and CO_2 in the middle ultraviolet (MUV) (Lee et al., 2019).

Using the aforementioned large vacuum chamber housing an electron gun system and the Mars Atmosphere and Volatile EvolutioN (MAVEN) mission Imaging UltraViolet Spectrograph (IUVS) Optical Engineering Model (OEM) instrument, we have obtained calibrated spectral measurements of the LBH band system from 125–175 nm over a range of lines-of-sight to capture most of the optical emissions within the LBH band system (McClintock et al., 2015). The experimental apparatus for emission cross sections has been discussed in detail previously (Ajello et al., 2017; Kanik et al., 2003; Noren et al., 2001).

The experiment reported here for N_2 passed an electron beam through a static gas at three different pressures: 5×10^{-6} Torr, 1×10^{-5} Torr, and 5×10^{-5} Torr, hereafter low, medium, and high, respectively, corresponding to N_2 abundances in the terrestrial atmosphere at altitudes of 125 km ($n = 1.8 \times 10^{11}$ cm^{-3}), 120 km ($n = 3.5 \times 10^{11}$ cm^{-3}), and 110 km ($n = 1.8 \times 10^{12}$ cm^{-3}). The IUVS-OEM measured the glow profile produced around the electron beam. Ideally, an infinitely long electron beam will produce a cylindrically uniform glow region, wherein single-scattering emission and excitation rates per unit length of the beam are equal with dipole-allowed electronic transitions occurring on the electron beam axis and metastable transitions forming an extended cylindrically symmetric glow. A large vacuum chamber, referred to as the Multi-Optical Beam Instrument (MOBI), is large enough to approximate this condition with its 1.5 m diameter girth and 2.35 m length. In the present work, the IUVS-OEM instrument was placed on a vertical moving stage with the entrance slit orthogonal to the electron beam table, peering at the electron beam up to 400 mm from the electron beam axis to fully measure both allowed and forbidden transitions. The electron-impact-fluorescence apparatus installed in the MOBI chamber consisted of an electrostatic electron gun source and Faraday cup separated by ~1/3-m, two large pair of Helmholtz coils surrounding the chamber, a static gas source, and the IUVS-OEM. For clarity of understanding we show the experimental apparatus in Figure 1, which is fully described in our earlier work (Ajello et al., 2017).

With a staged three-step motion, the field-of-view (FOV) of the IUVS-OEM detector was projected to more than 400 mm object vertical distance at the electron beam allowing the observation of metastable emissions. Three overlapping images were taken at different stage positions to capture the glow region from long-lived states such as $N_2\ a\ ^1\Pi_g$. We can vary the vertical height of the placement of the optic axis of the IUVS-OEM at three positions above the electron beam axis. We start from Image-1 on center ($z = 0$) with the emission from dipole-allowed transitions centered near spatial pixel 500, followed by a motion in the z-direction to obtain

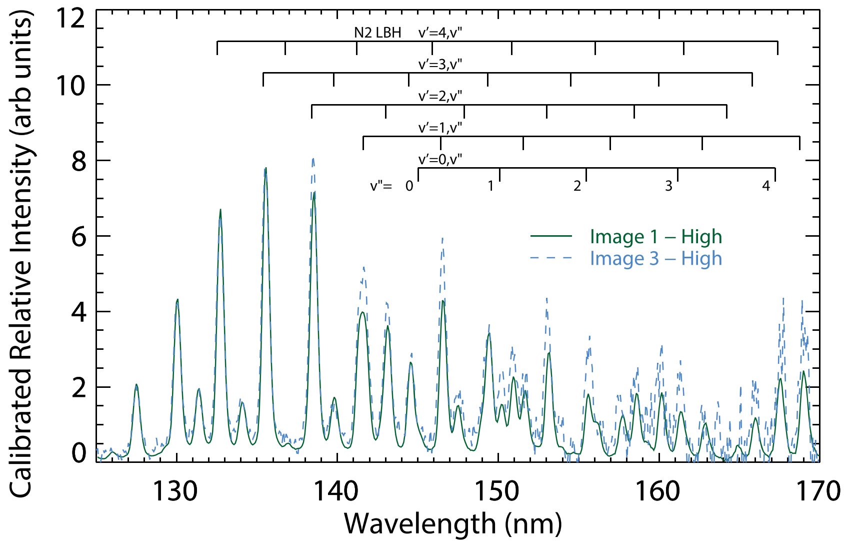

Figure 2. The electron impact fluorescence spectra at 30 eV from N_2 for Image-1 and Image-3 at high gas pressure of 5×10^{-5} Torr with an electron beam current of ~80 μA. The radial glow pattern extends from beam center at 0 mm to 400 mm. IUVS-OEM optic axis in vertical position with respect to the electron beam is centered 30.48 cm (12 inches) above the electron beam axis for Image-3. The two spectra are normalized to the LBH a(3,0) band at 135.4 nm. The LBH v′, v″ = 0, 1, 2, … progressions for v′ = 0, 1, 2, 3, 4 are indicated in the figure.

Image-2 centered at 15.24 cm (6 inches), and Image-3 centered at 30.48 cm (12 inches) above the electron beam. The total vertical object size in the MOBI chamber imaged by the central 810 spatial pixels of the IUVS-OEM is 16.4 cm with Image-1 positioned at the center of the FOV. The same set of three spatial image positions is used at low, medium, and high pressure. The set of 810 pixels used is a subset of the full 1024 pixels and is chosen to avoid the pixels of the broad occultation keyholes at each end of the slit, which are used on the flight instrument for stellar occultation observations.

Our main discussion in this paper involves an analysis of the best-fit LBH vibrational intensities for the Image-1 and Image-3 laboratory measured spectra, for example, Image-1 low pressure or Image-1 high pressure compared to Image-3 high pressure. These conditions present different spectra, as evidenced in Figure 2, where we have overplotted the high-pressure spectra for Image-1 and Image-3 with both spectra normalized to the a(3,0) band at 135.4 nm. Multiple Linear Regression (MLR) glow model fits to the measured 100 eV medium, and high pressure FUV intensities for the portion of the LBH spectrum from 133.5–140.2 nm, a spectral region devoid of N I features, are shown in Figures 3a and 3b, respectively. Both sets of glow patterns show that only Image-1 captures a direct excitation spectrum with termination of direct excitation photons in the model, shown in green near 10 cm radial distance from the electron beam. The Image-3 glow pattern in the model, shown in magenta, captures the cascade-induced LBH spectrum, which dominates from radial distances of 22.5–38.5 cm.

An important diagnostic of the IUVS-OEM optical performance in the laboratory requires a measurement of the point-spread function (PSF). To obtain the PSF, the MOBI chamber background gas consisting of predominantly H_2O, following pump-down, was sampled at an approximately static pressure of ~7×10^{-6} Torr for a short duration, and the electron gun provided an electron beam current of ~30 μA. The FUV spectrum of electron impact fluorescence of H_2O is very simple, composed of mostly H I Lyman-α and O I (115.2, 130.4, and 135.6 nm) emission features (Ajello & Shemansky, 1985). The model fit, f, to the PSF is given in Ajello et al. (2019).

3. The Spectral Analysis

For diatomic molecules in an electronically excited state, the number of photons emitted per unit volume per second in a transition from the v′ upper vibrational level to the v″ lower vibrational level (Beegle et al., 1999), referred to as the electronic band emission rate, is

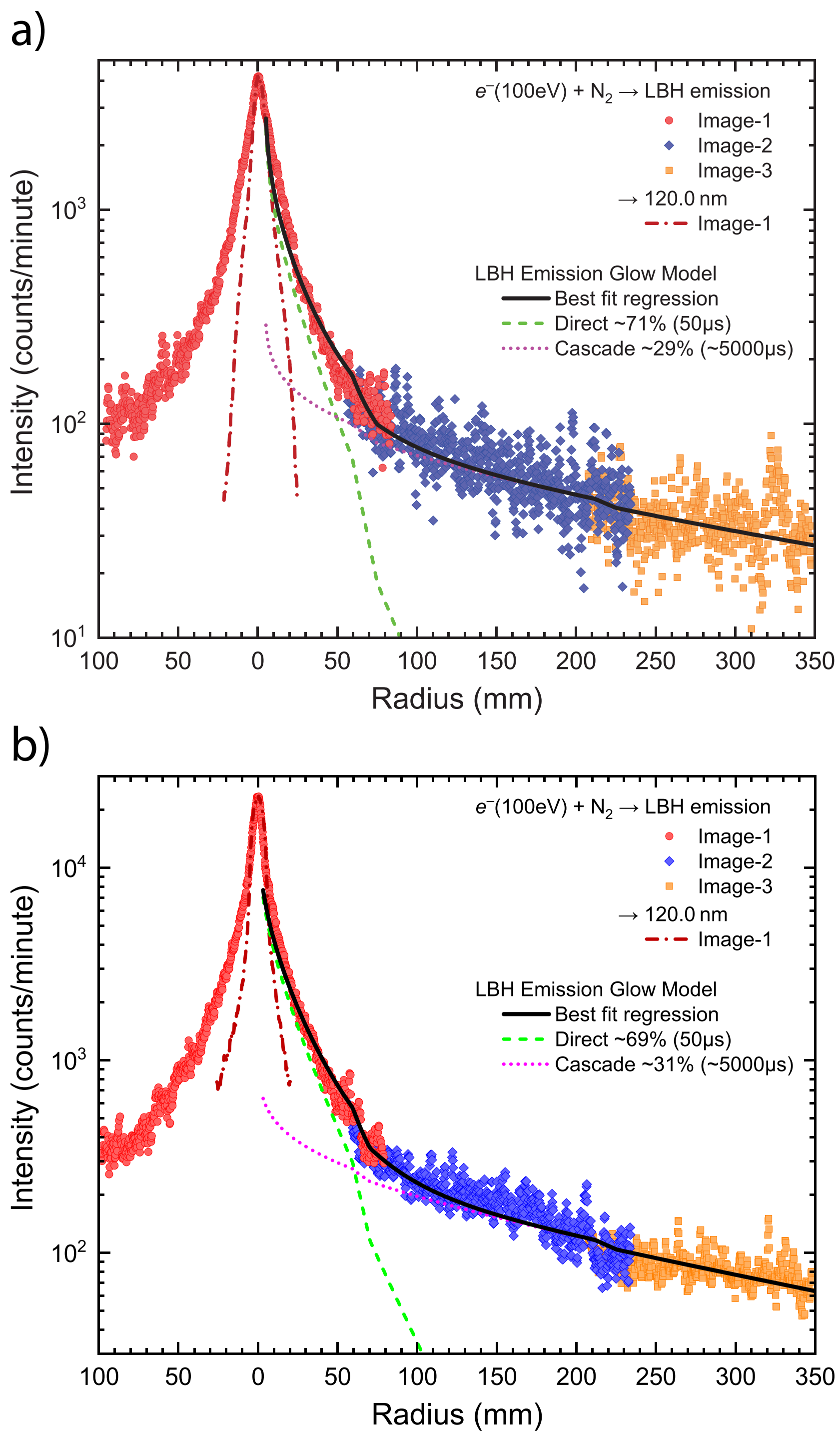

Figure 3. A glow model composed of two lifetimes that is the best MLR fit of the glow data at 100 eV electron impact energy with (a) medium pressure and (b) high pressure and an electron beam current of ~150 μA. The MLR ascertains two best-fit direct excitation lifetimes: for direct excitation (~50 μs) to the $a\ ^1\Pi_g$ state in green and for cascade-induced excitation (~5000 μs) from the ($a'^1\Sigma_u^-$ and $w^1\Delta_u \rightarrow a^1\Pi_g \rightarrow X^1\Sigma_g^+$) states to the a-state in magenta. We show the best model regression fits for the two lifetimes in black for each glow. Both sets of glow patterns show that only Image-1 captures a direct excitation spectrum with termination of direct excitation photons in the model, shown in green, near 10 cm radial distance from the electron beam. The Image-3 glow pattern in the model, shown in magenta, captures the cascade-induced LBH spectrum, which dominates from radial distances of 22.5–38.5 cm.

Table 1
Relative Electronic Band Emission Vibrational Intensities at 30 eV

		Image-1			Image-3		
Vibrational v′-level	FC factor	Low pressure	Medium pressure	High pressure	Low pressure	Medium pressure	High pressure
0	0.043	0.040	0.038	0.037	0.087	0.068	0.061
1	0.116	0.114	0.112	0.108	0.135	0.142	0.144
2	0.171	0.167	0.168	0.163	0.179	0.178	0.173
3	0.183	0.183	0.181	0.177	0.177	0.170	0.165
4	0.160	0.157	0.160	0.163	0.136	0.141	0.147
5	0.122	0.126	0.127	0.131	0.097	0.102	0.114
6	0.083	0.091	0.091	0.098	0.066	0.077	0.073
Total	0.877	0.878	0.877	0.877	0.877	0.878	0.877

$$\mathrm{I}_{\mathrm{v}'\mathrm{v}''} = \mathrm{p}_{\mathrm{v}'}\mathrm{A}_{\mathrm{v}'\mathrm{v}''}/\mathrm{A}_{\mathrm{v}}, \tag{1}$$

where $\mathrm{p}_{\mathrm{v}'}$ is the volumetric excitation rate for the v′ level of the upper electronic state, and $\mathrm{A}_{\mathrm{v}'\mathrm{v}''}$ and $\mathrm{A}_{\mathrm{v}'}$ are the vibrational and total transitional probabilities for each v′ level to a lower electronic state. The value $\mathrm{p}_{\mathrm{v}'}$ is defined by

$$\mathrm{p}_{\mathrm{v}'} = \mathrm{F_e N_0}\left(\sigma_{\mathrm{excitation}}{}^{\mathrm{v}'} + \sigma_{\mathrm{cascade}}{}^{\mathrm{v}'}\right), \tag{2}$$

where $\mathrm{F_e}$ is the electron flux, $\mathrm{N_0}$ is the gas density (cm^{-3}), $\sigma_{\mathrm{excitation}}{}^{\mathrm{v}'}$ is the excitation cross section (cm^2), and $\sigma_{\mathrm{cascade}}{}^{\mathrm{v}'}$ is the total cascade cross section (cm^2) to level v′ of the *a*-state from various vibrational levels of the *a*′- and *w*-states. Note that $\sigma_{\mathrm{excitation}}{}^{\mathrm{v}'}$ is proportional to $\mathrm{q}_{\mathrm{v}'0}\,\mathrm{R_e}^2(\mathrm{r}_{\mathrm{v}'0})$, where $\mathrm{q}_{\mathrm{v}'0}$ is the Franck-Condon factor (FCF) from ground vibrational level to v′, $\mathrm{r}_{\mathrm{v}'0}$ is the corresponding internuclear distance, and $\mathrm{R_e}^2$ is the square of the electronic transition moment. Also note that we have previously shown dipole-allowed cascade from three Rydberg series, with lowest members $b^1\Pi_u, c_3{}^1\Pi_u, o_3{}^1\Pi_u, b'^1\Sigma_u^+$, and $c_4'^1\Sigma_u^+$, as well as valence-type states, is small (Heays et al., 2014). There is less than 5% variation of the electronic transition moment, $\mathrm{R_e}$, of the *a*-state (Ajello, 1970), so the variation of $\mathrm{R_e}$ with internuclear distance can be neglected.

We use MLR techniques to fit an N_2 LBH band emission rate model (Budzien et al., 1994) to each IUVS-OEM measurement obtained in our laboratory experiment. The PSF (discussed above) was used to spectrally smear individual molecular rotational lines to model the measured electron impact fluorescence FUV spectra. The measured laboratory temperature established the rotational temperature of 293 K when fitting spectra with the band model. With the exception of the N I 149.3 nm doublet, which was removed from the measured spectra prior to fitting, expected atomic multiplets (N, H, and O, the latter two resulting from residual gas in the tank) were included as source components in the fits. Uncertainties in the measured spectra are propagated through the MLR fit when obtaining coefficients (i.e., v′-vibrational populations) and their corresponding uncertainty estimates. In Table 1 we list the MLR band emission rate model results for the six spectra of Images-1 and -3. The observed pre-dissociation of the *a*-state for rotational levels above v′ = 6, J = 13 accounts for 12.3% of the excitation cross section resulting in emission from v′ > 6 to be weak or absent (Ajello, 1970). Thus, the total probability for emission for all columns in Table 1 has been normalized to $\sum_{\mathrm{v}'}^{6}\mathrm{q}_{\mathrm{v}'0} = 0.877$.

In Figure 4a (bottom abscissa, left ordinate) we show the IUVS-OEM electron-excited 30 eV Image-1 laboratory spectra at a radial distance of 0 cm from the electron beam for low and high pressure. The spectra are normalized to the LBH *a*(3,0) band at 135.4 nm. Also shown in the figure (top abscissa, right ordinate) is a comparison of direct excitation theoretical Franck-Condon factors, $\mathrm{q}_{\mathrm{v}'0}$, from Loftus and Krupenie (1977) with vibrational intensities for each v′ (0,1,2, … ,6), v″-progression from MLR fits to Image-1 spectra at low and high pressure, and a fit to the Image-3 spectrum at high pressure. The low v′ levels 0, 1, and 2 are enhanced in Image-3, which exhibits a cascade spectrum for a gas pressure of 5×10^{-5} Torr, equivalent to an N_2 gas density of 1.8×10^{12} cm^{-3}. The enhancement of the strong *a*(1,1) band at 146.4 nm is very noticeable in Figure 2. This N_2 density occurs at terrestrial altitudes near 110–115 km, well below the dayglow peak of the LBH emission rate near 150 km. The v′ = 0 level is the most enhanced by combined CIET and radiative processes by almost 50% when comparing vibrational intensities for Image-1 and Image-3 at high pressure.

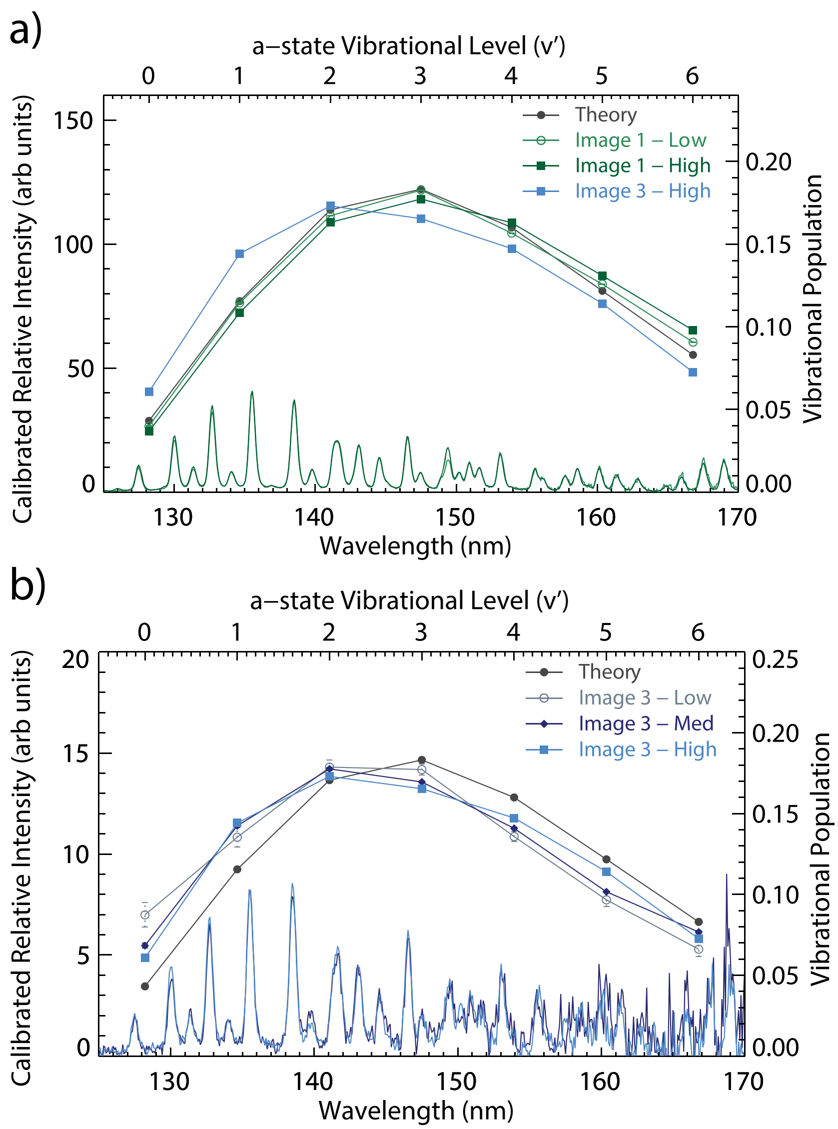

Figure 4. (a) (Bottom abscissa, left ordinate) IUVS-OEM electron-excited 30 eV Image-1 laboratory spectra are centered on the electron beam axis at a radial distance of 0 cm from the electron beam at low (light green) and high (dark green) pressure. The spectra are normalized to the LBH a(3,0) band at 135.4 nm. The difference between the two spectra near 149 nm is due to pressure dependence of the N I 149.3 nm emission. (Top abscissa, right ordinate) Comparison of the v′-vibrational populations from a Franck-Condon based theoretical model (filled circles) (Ajello, 1970; Ajello & Shemansky, 1985; Heays et al., 2014; Loftus & Krupenie, 1977) with v′-vibrational populations from MLR fits to Image-1 spectra at low (open circles) and high pressure (green squares) and an Image-3 spectrum at high-pressure (blue squares). Vertical uncertainty bars for fitted v′-vibrational populations are included in the plot but are not readily evident because the signal-to-noise ratio of the laboratory measurements is large (see section 4 and Figure 7). (b) (Bottom abscissa, left ordinate) IUVS-OEM electron-excited 30 eV Image-3 laboratory spectra at a radial distance of 30.48 cm from the electron beam for medium (dark purple) and high (light blue) pressure. The spectra are normalized to the LBH a(3,0) band at 135.4 nm. (Top abscissa, right ordinate) Comparison of the v′-vibrational populations from a Franck-Condon based theoretical model (filled circles; same as used for Figure 4a) with v′-vibrational populations from MLR fits to Image-3 spectra at low (open circles), medium (diamonds), and high (squares) pressures.

The results of an MLR analysis comparing vibrational intensities of Image-3 at low, medium, and high pressures are shown in Figure 4b (top abscissa, right ordinate). IUVS-OEM electron-excited 30 eV Image-3 laboratory spectra at a radial distance of 30.48 cm from the electron beam for medium and high pressures are also shown (bottom abscissa, left ordinate). The spectra are normalized to the LBH a(3,0) band at 135.4 nm. The airglow observations reported by Budzien et al. (1994), and the CIET model

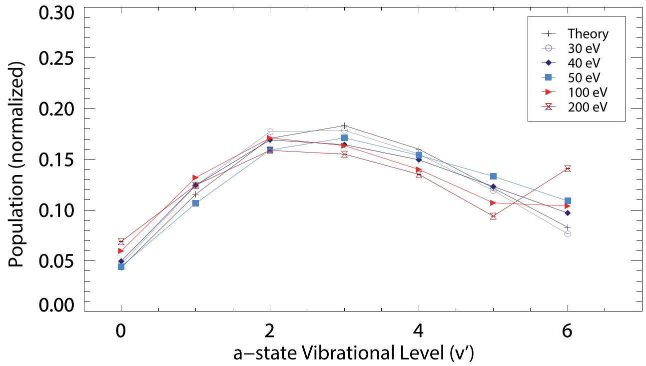

Figure 5. The v′-vibrational populations from MLR fits to the sum of Images 1–3 spectra at high pressure (blue squares) at electron impact energies between 30 and 200 eV. As in Figure 4, uncertainties in the measured spectra are propagated through the MLR fit when obtaining v′-vibrational populations and their corresponding uncertainty estimates, which are shown as vertical bars in the figure (not readily evident).

results of Eastes (2000), expected for airglow rocket observations at a tangent altitude of 200 km, indicate similar enhancements in the low vibrational levels evident in our Image-3 high-pressure spectrum. We expect to see this enhancement in any N_2 FUV limb spectra of the dayglow at the reference altitudes used in our laboratory experiment. Even in the absence of a significant collision rate (e.g., ~0.1 s^{-1}) as expected near 200 km (n~3.6 × 10^9 cm^{-3}), the radiative induced-cascade from the $a'^1\Sigma_u^-$ and $w^1\Delta_u \rightarrow a^1\Pi_g \rightarrow X^1\Sigma_g^+$) states will take place in our experiment with a larger transition probability (~10^3 s^{-1}) than the collision rate due to deactivation that takes place in the lab with a small chamber (Gilmore et al., 1992).

Low-v′ enhancement for medium and high pressures was recognized in the LBH intensity versus pressure variation studies in the work of Ajello (1970) and Holland (1969) with a small vacuum chamber compared to the MOBI chamber at CU. In these earlier experiments, only *Image-1*-type spectra were possible, requiring higher pressures to see CIET than obtained here for our low-pressure Image-3 measurements.

The strength of the radiative-CIET cascade process induced low-v′ enhancement is expected to increase with gas pressure. This is because the CIET process, strictly speaking, is a secondary collision in this experiment via the processes in equation (3) between excited states but is not, strictly speaking, single-scattering:

$$\mathrm{N_2}\left(a'^1\Sigma_u^-, w^1\Delta_u, a^1\Pi_g\right) + \mathrm{N_2}\left(X^1\Sigma_g^+\right) \leftrightarrow \mathrm{N_2}\left(a'^1\Sigma_u^-, w^1\Delta_u, a^1\Pi_g\right) + \mathrm{N_2}\left(X^1\Sigma_g^+\right). \quad (3)$$

Eastes and Dentamaro (1996) and Freund (1972) have indicated that the following radiative and CIET collisions occur interchangeably: $a \leftrightarrow a'$, $w \leftrightarrow a$, with no coupling between the *w*- and *a′*-states. Marinelli et al. (1989) and Katayama et al. (1994) have shown a strong exothermic reaction for $a(\mathrm{v}' = 0) \rightarrow a'(\mathrm{v}' = 0)$ should be the dominant contribution to the CIET rate constant as we verify in this experiment.

4. Discussion

In order to demonstrate the separation of the two types of LBH spectra, we performed a best-fit MLR for the 100 eV medium and high-pressure glow patterns employing a direct excitation lifetime and a composite cascading lifetime as in Figure 3. Direct excitation becomes insignificant (<1%) at distances greater than 10 cm from the electron beam. We found a similar result for all energies from 30–200 eV. The regression analysis showed a physically meaningful direct excitation model for the fast component lifetime of ~50 μs and ~5000 μs for the cascade-induced LBH spectrum, similar to the 100 eV spectrum studied in Ajello et al. (2017). The observed ratio of direct excitation to cascade-induced excitation to the *a*-state in this experiment is nominally ~70% to ~30% for all energies above 30 eV.

Direct excitation observed in the set of three Image-1 at all pressures for all our laboratory spectra at 30 eV are nearly identical and can all be closely modeled with Franck-Condon factors, though the trends in Table 1 for Image-1 relative to theory suggest a pressure dependence in the retrieved vibrational intensities. Cascading processes observed in Image-3 at high pressure result in a large increase in the LBH emission intensity at electron collision energies of 10–200 eV, which also corresponds to the typical energy range for secondary electrons in Earth's upper atmosphere. The LBH band emission rate from cascade varies with gas pressure with main enhancement to low v′ levels. The cross section for cascading-induced LBH emission is found to be pressure dependent and also energy dependent as discussed in the past (Eastes & Dentamaro, 1996). We show in Figure 5 the relative LBH vibrational band intensities for Image-3 as a function of energy normalized to 0.877, the sum of FCF ($q_{\mathrm{v}'0}$) for emission. CIET effects become stronger with increasing energy for the sum of Images-1 to -3 at high pressure. The trend in fitted populations for v′ = 6 is not understood at present and will require further investigation.

We display in Figure 6 and tabulate in Table 2 the variation of LBH direct emission cross section and LBH cascade-induced emission cross section with energy measured in this experiment at 40, 50, 100, and 200 eV

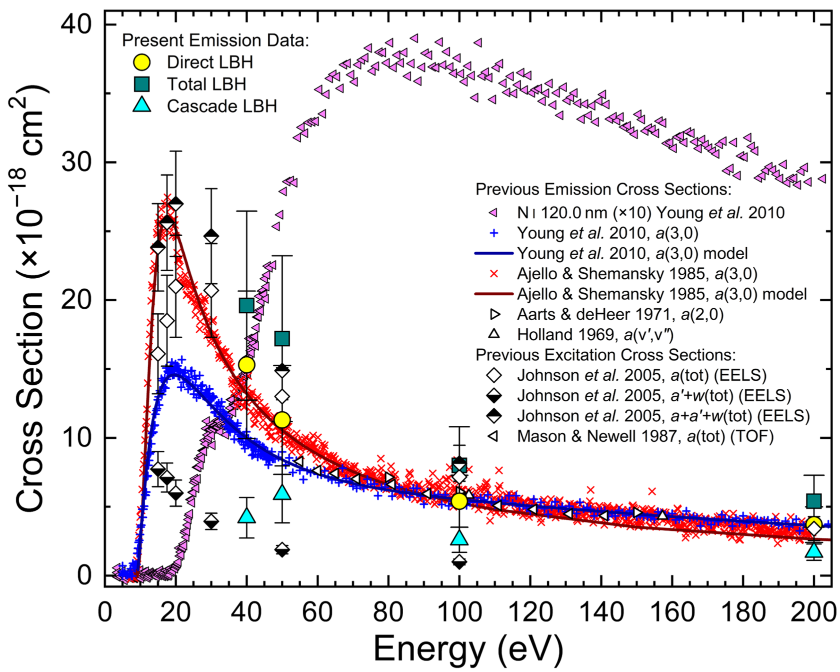

Figure 6. The LBH direct, cascade and total emission cross sections as a function of energy are the medium pressure absolute cross sections. We also show a comparison of the excitation function of this experiment to the direct LBH emission cross section measurements of Ajello and Shemansky (1985) and Young et al. (2010) normalized to the 100 eV direct emission cross section of 5.4×10^{-18} cm^2 of this measurement. The previous LBH emission cross section work of Aarts and de Heer (1971) and Holland (1969), as well as the LBH excitation cross section work of Mason and Newell (1987), from a time-of-flight (TOF) experiment, and the excitation integral cross sections (ICSs) of Johnson et al. (2005), from electron energy loss spectroscopy (EELS) results, are also displayed in the figure. The a'- and w-state ICSs of Johnson et al. were summed and plotted, which are an effective cascade-induced emission cross section, along with the summation with the a-state ICS, thus representing an effective total excitation cross section, $a + a' + w$.

at medium pressure. The N_2 LBH emission cross section at each energy is normalized relative to the N I 120.0 nm emission cross sections of Ajello and Shemansky (1985) with the correction factor suggested by Malone et al. (2008): at 100 eV, $\sigma_{120.0\ nm} = 3.70 \times 10^{-18}$ cm^2. The *Ajello et al.* emission cross sections are nearly identical to Young et al. (2010) (for example, see Figure 3 in Young et al., 2010). The medium pressure LBH direct-emission and cascade-emission cross sections in Table 2 are averaged based on the 100 eV direct LBH emission cross section results of Ajello et al. (2017) for 100 eV of 6.4 $\times 10^{-18}$ cm^2 and the 100 eV direct LBH emission value measured in this new experiment at medium pressure of 4.3×10^{-18} cm^2, resulting in a 100 eV LBH direct emission cross section of 5.4×10^{-18} cm^2. Previously measured direct LBH emission cross sections in Figure 6 at 100 eV are normalized to this value. The averaged emission cross section results in Table 2 show cascading accounts for ~30% ($\sigma^{em}{}_{casc} = 2.6 \times 10^{-18}$ cm^2) of the glow pattern, and direct excitation of the a-state provides ~70% of the LBH emission ($\sigma^{em}{}_{dir} = 5.4\times 10^{-18}$ cm^2, i.e., the typical "laboratory" LBH cross section for smaller

Table 2
Measured LBH Emission Cross Sections

Energy (eV)	Total emission cross section (10^{-17} cm^2)	Direct emission cross section (10^{-17} cm^2)	Cascade emission cross section (10^{-17} cm^2)	Predissociation cross section (10^{-17} cm^2)	Excitation cross section (10^{-17} cm^2)
40	1.95	1.53	0.42	0.21	1.74
50	1.72	1.13	0.59	0.16	1.29
100	0.80	0.54	0.26	0.08	0.62
200	0.54	0.37	0.17	0.05	0.42

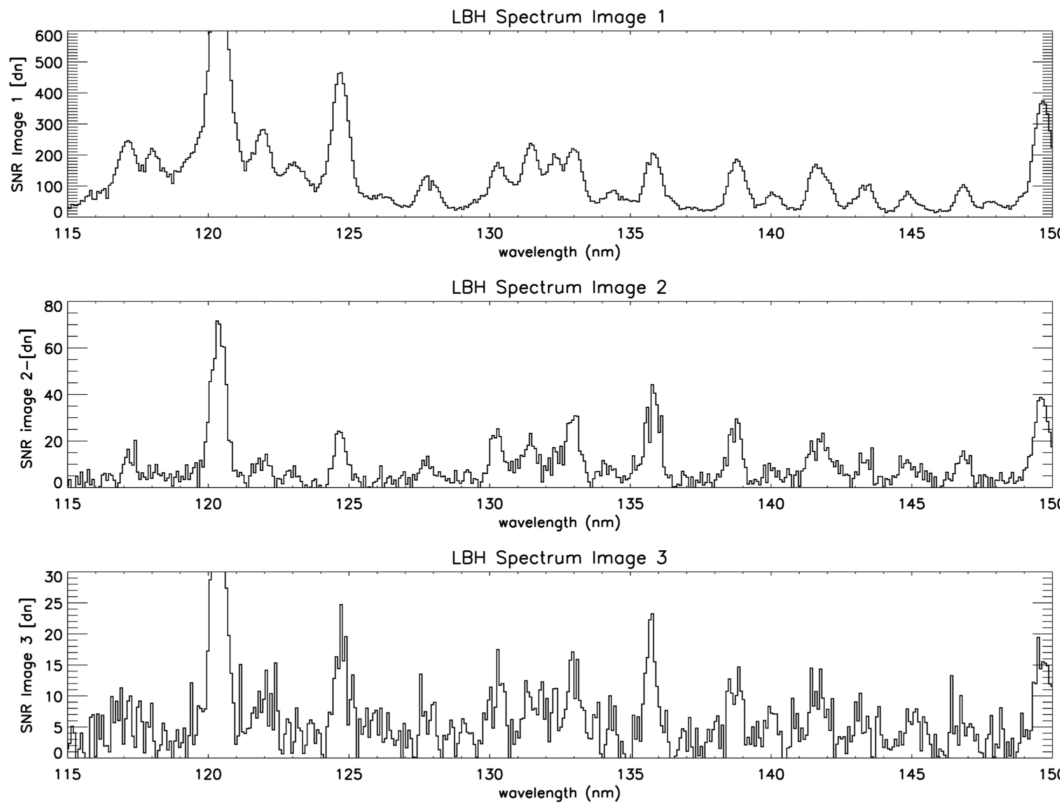

Figure 7. Statistical SNR used to determine the 100 eV emission cross sections in Table 2 and Figure 6 plotted as the ratio of the summed total signal counts, less background counts, of the raw data in all 65 s frame intervals for each of the three images (364 in number for Image-1 at 100 eV medium pressure). This was acquired over 8–10 hr divided by the background noise defined as the square root of the sum of the squares of the standard deviation of dark counts for each of the dark-acquiring frames and the standard deviation of light counts of signal for each of the 65 s light-acquiring frames described in Ajello et al. (2017, 2019).

FOV setups). Thus, the total LBH emission cross-section is $\sigma^{em}{}_{total} = 8.0\times 10^{-18}$ cm^2, which is effectively the "aeronomical" LBH cross-section at 100 eV. We also list in Table 2 the LBH predissociation cross sections and excitation cross sections as calculated in Ajello et al. (2017).

The composite uncertainty of the 100 eV (LBH) band system ($a^1\Pi_g \rightarrow X^1\Sigma_g^+$) emission cross section values is ~35% including the statistical uncertainty of the signal-to-noise ratio (SNR). The uncertainty of our work is the root-sum-square uncertainty of (1) ~15% in the relative FUV calibration, (2) ~13.5% uncertainty of the absolute calibration of N I 120.0 nm, (3) ~5% uncertainty in the Faraday cup current loss to the grounded shield, (4) ~5% uncertainty to pressure drift, (5) ~15% uncertainty in measured areas from blended feature overlap, (6) ~20% uncertainty for the cascade-induced emission beyond ~400 mm radius from electron beam, and (7) SNR statistical uncertainty of 10%.

We show the statistical uncertainties in Figure 7 for Images 1–3 for the wavelength region of the spectrum used for the emission cross section determination. The SNR remains >5 for all three of the images in the wavelength range. This wavelength range of 133.5–140.0 nm contains only LBH bands representing ~13.5% of the band system without any contamination from atomic-N multiplets, and we use the integrated intensity (i.e., intensities summed over positive z-translation above the electron beam from 0–400 mm) from this portion of the LBH band system to deduce the cross section of the band system (Ajello & Shemansky, 1985). The two strongest bands of the LBH system dominate this spectral range: the a(2,0) and a(5,3) bands at 138.3 nm and the a(3,0) and a(6,2) bands at 135.3 nm. In addition, we included in this interval the a(5,1) band at 133.9 nm and the a(6,3) and a(3,1) bands at 139.5 nm. We determine from glow models that we were able to measure >98% of the emitted photons in the 133.5–140.0 nm spectral interval that arise from direct excitation.

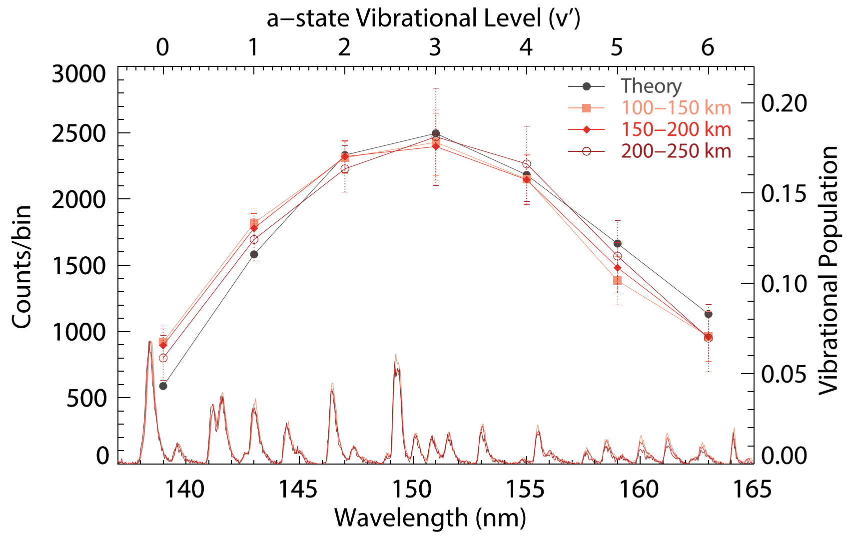

Figure 8. (Bottom abscissa, left ordinate) GOLD observed spectra summed in 50 km tangent altitude bins covering 100–150, 150–200, and 200–250 km. The spectra are normalized to the LBH *a*(2,0) band at 138.3 nm. (Top abscissa, right ordinate) Comparison of the v′-vibrational populations from a Franck-Condon based theoretical model (filled circles; same as used for Figure 4) with v′-vibrational populations from MLR fits to the GOLD observed spectra at altitude bins covering 100–150 km (squares), 150–200 km (diamonds), and 200–250 km (open circles).

A recent example of the CIET effect in planetary atmospheres can be seen in MLR fits to observations by the Global-scale Observations of the Limb and Disk (GOLD) instrument. Figure 8 (top abscissa, right ordinate) shows vibrational intensities from MLR fits to limb FUV observations made on 31 October 31 2018. The observed spectra have been summed over three altitude ranges: 100–150 km, 150–200 km, and 200–250 km. Similar to the approach used for the laboratory-measured spectra, the GOLD PSF was used to spectrally smear individual molecular rotational lines to model the observed FUV spectra. When fitting the GOLD spectra, the effective rotational temperature (~840 K) was first obtained using Powell optimal estimation techniques. The observed spectra for the three altitude bins, normalized to the *a*(2,0) band at 138.3 nm, are also shown in Figure 8 (bottom abscissa, left ordinate). As done with the laboratory-measured spectra, the N I 149.3 nm doublet was removed from the measured spectra prior to fitting; no atomic multiplets were included as source components in the fits. There is a clear low-v′ enhancement in all three altitude-bins, less so from 200–250 km, an indication of pressure dependent CIET effects. Two distinct trends are noted: lower altitudes where collisional contributions dominate and higher altitudes where radiative cascade dominates.

5. Summary

We have measured the LBH cascade-induced spectra at 30–200 eV for three different N_2 gas pressures corresponding to terrestrial altitudes between 110 and 125 km (airglow) and at three different imaging glow distances from the electron beam of 0, 15.24 (6 in), and 30.48 cm (12 in). The cascade-induced UV spectra were obtained from an LBH glow laboratory measurement generated by an electron beam in a large vacuum chamber. Image-1 solely contains the electron beam spectrum, and Image-3 at 30.48 cm distance from the electron beam captures only the cascade spectrum.

The LBH emission cross section variation with both pressure and energy must be further studied at lower energy near to threshold (~8.55 eV) than the 40–200 eV energy range measured here for input into state-of-the-art electron transport models for accurate dayglow and auroral analysis. The previous low energy studies of the LBH direct emission cross section, albeit in a small chamber, were performed by Ajello and Shemansky (1985) and Young et al. (2010). We show these excitation function measurements for direct emission in Figure 6, normalized at 100 eV to the direct emission cross section value of 0.54×10^{-17} cm^2 measured here. The renormalized previous LBH emission cross section work of Aarts and de Heer (1971) and Holland (1969), as well as the LBH excitation cross section work of Mason and Newell (1987) and Johnson et al. (2005), are also displayed in the figure.

The revised Ajello and Shemansky direct emission cross sections in Figure 6 agree closely with the peak cross section values tabulated in the review article of Ajello et al. (2011). Ajello et al. (2011) indicate in their table 28.5 a peak total LBH direct emission cross section of 2.65×10^{-17} cm^2 at 18 eV. The review article includes a discussion of the work of Eastes (2000) and Budzien et al. (1994) from terrestrial dayglow observations. The latter two publications indicate peak total emission cross sections including cascade-induced emission cross section of 2.9×10^{-17} cm^2 and 3.55×10^{-17} cm^2 at 18 eV, respectively. These direct and total peak emission cross section values at 18 eV are in excellent agreement with the peak direct emission cross section value indicated in Figure 6 for the revised work of Ajello and Shemansky of ~2.9×10^{-17} cm^2. Until we can build an electrostatic gun that can operate at low electron acceleration energy of <30 eV we recommend adoption of a 30% contribution to the total emission cross section from cascade-induced LBH emission at all energies above ~30 eV, where vibrational level threshold effects are negligible.

Acknowledgments

This work was performed at the Laboratory for Atmospheric and Space Physics (LASP), University of Colorado (CU) Boulder, and the Jet Propulsion Laboratory (JPL), California Institute of Technology (Caltech), under a contract with the National Aeronautics and Space Administration (NASA). We gratefully acknowledge financial support through NASA's Solar System Workings, Cassini Data Analysis Program, the Heliophysics HTIDES and Geospace Science programs, and the National Science Foundation Aeronomy Program Office. This research was also supported by NASA through the MAVEN project including the use of the IUVS-OEM. R. A. Lee thanks the NSF Research Experiences for Undergraduates (REU) program for support. We thank Karl Hubbell for technical support. The GOLD data used in this analysis are available through the NASA Space Physics Data Facility (https://cdaweb.gsfc.nasa.gov/pub/data/gold/).

References

Aarts, J. F. M., & de Heer, F. J. (1971). Emission cross sections for NI and NII multiplets and some molecular bands for electron impact on N_2. *Physica*, *52*, 45–73. https://doi.org/10.1016/0031-8914(71)90036-X

Ajello, J., Malone, C., McClintock, W., Hoskins, A., & Eastes, R. (2017). Electron impact measurement of the 100 eV emission cross section and lifetime of the Lyman-Birge-Hopfield Band System of N_2: Direct excitation and cascading. *Journal of Geophysical Research: Space Physics*, *122*, 6776–6790. https://doi.org/10.1002/2017JA024087

Ajello, J. M. (1970). Emission cross sections of N_2 in the vacuum ultraviolet by electron impact. *The Journal of Chemical Physics*, *53*(3), 1156–1165. https://doi.org/10.1063/1.1674113

Ajello, J. M., Malone, C. P., Evans, J. S., Holsclaw, G. M., Hoskins, A. C., Jain, S., et al. (2019). UV study of the Fourth Positive Band System of CO and OI 135.6 nm from electron impact of CO and CO_2. *Journal of Geophysical Research: Space Physics*, *124*, 2954–2977. https://doi.org/10.1029/2018JA026308

Ajello, J. M., Mangina, R. S., & Meier, R. R. (2011). UV Molecular Spectroscopy from Electron Impact for Applications to Planetary Atmospheres and Astrophysics. In Y. Hatano, Y. Katsumura, & A. Mozumder (Eds.), *"Charged Particle and Photon Interactions with Matter" Recent Advances, Applications, and Interfaces* (chapter 28, pp. 761–804). Boca Raton: Taylor & Francis.

Ajello, J. M., & Shemansky, D. E. (1985). A reexamination of important N_2 cross sections by electron impact with application to the dayglow: The Lyman-Birge Hopfield Band System and NI (119.99 nm). *Journal of Geophysical Research*, *90*(A10), 9845–9861. https://doi.org/10.1029/JA090iA10p09845

Beegle, L., Ajello, J. M., James, G. K., Dziczek, D., & Alvarez, M. (1999). The emission spectrum of the CO ($A\ ^1\Pi$ - $X\ ^1\Sigma^+$) Fourth Positive System by electron impact. *Astronomy and Astrophysics*, *346*, 375–390.

Budzien, S. A., Feldman, P. D., & Conway, R. R. (1994). Observations of the far ultraviolet airglow by the Ultraviolet Limb Imaging experiment on STS-39. *Journal of Geophysical Research*, *99*(A12), 23,275–23,287. https://doi.org/10.1029/94JA01543

Cartwright, D. (1978). Vibrational populations of the excited states of N_2 under auroral conditions. *Journal of Geophysical Research*, *83*, 517–531. https://doi.org/10.1029/JA083iA02p00517

Eastes, R. W. (2000). Modeling the N_2 Lyman-Birge-Hopfield bands in the dayglow: Including radiative and collisional cascading between the singlet states. *Journal of Geophysical Research*, *105*(A8), 18,557–18,573. https://doi.org/10.1029/1999JA000378

Eastes, R. W., & Dentamaro, A. V. (1996). Collision-induced transitions between the $a\ ^1\Pi_g$, $a'\ ^1\Sigma_u^-$, $w\ ^1\Delta_g$ states of N_2: Can they affect auroral N_2 Lyman-Birge-Hopfiled band emissions? *Journal of Geophysical Research*, *101*, 26,931–26,940. https://doi.org/10.1029/96JA01636

Evans, J. S., Strickland, D. J., & Huffman, R. E. (1995). Satellite remote sensing of thermospheric O/N_2 and solar EUV, 2. Data analysis. *Journal of Geophysical Research*, *100*(A7), 12,227–12,233.

Freund, R. S. (1972). Radiative lifetime of N_2 ($a\ ^1\Pi_g$) and formation of metastable N_2 ($a'\ ^1\Sigma_u^-$). *The Journal of Chemical Physics*, *56*(9), 4344–4351. https://doi.org/10.1063/1.1677870

Gilmore, F. R., Laher, R. R., & Espy, P. J. (1992). Franck-Condon factors, r-centroids, electronic transition moments, and Einstein coefficients for many nitrogen and oxygen band systems. *Journal of Physical and Chemical Reference Data*, *21*(5), 1005–1107. https://doi.org/10.1063/1.555910

Heays, A. N., Ajello, J. M., Aguilar, A., Lewis, B., & Gibson, S. T. (2014). The high resolution EUV spectrum of N_2 by electron impact. *Astrophysical Journal Supplement*, *211*, 1–27. https://doi.org/10.1088/0067-0049/211/2/28

Holland, R. F. (1969). Excitation of nitrogen by electrons: The Lyman-Birge-Hopfield system of N_2. *The Journal of Chemical Physics*, *51*, 3940–3950. https://doi.org/10.1063/1.1672614

Johnson, P. V., Malone, C. P., & Kanik, I. (2005). Integral cross sections for the direct excitation of the $A\ ^3\sum_u^+$, $B\ ^3\prod_g$, $W\ ^3\Delta_u$, $B'\ ^3\sum_u^-$, $a'\ ^1\sum_u^-$, $a\ ^1\prod_g$, $w\ ^1\Delta_u$, and $C\ ^3\prod_u$ electronic states in N_2 by electron impact. *Journal of Geophysical Research*, *110*, A11311. https://doi.org/10.1029/2005JA011295

Kanik, I., Noren, C., Makarov, O., Vatti Palle, P., Ajello, J., & Shemansky, D. (2003). Electron impact dissociative excitation of O2. II. Absolute emission cross sections of OI(130.4 nm) and OI(135.6 nm). *Journal of Geophysical Research*, *108*(E11), 51256. https://doi.org/10.1029/2000JE001423

Katayama, D. H., Dentamaro, A. V., & Welsh, J. D. (1994). State specific electronic quenching rates for N_2 $a\ ^1\Pi_g(v = 0)$ level from collisions with He, Ar, and N_2. *The Journal of Chemical Physics*, *101*, 9422–9428. https://doi.org/10.1063/1.467973

Lee, R. A., Ajello, J. M., Malone, C. P., Holsclaw, G., Jain, S., McClintock, W. E., et al. (2019). Laboratory Aeronomy by Electron Impact of CO and CO2 for Analysis of UV Observations of the Martian Upper Atmosphere. AGU Fall Meeting abstract session P031 - Processes in the present-day Atmosphere of Mars, San Francisco, CA.

Loftus, A., & Krupenie, P. H. (1977). The spectrum of molecular nitrogen. *Journal of Physical and Chemical Reference Data*, *6*, 113–307. https://doi.org/10.1063/1.555546

Malone, C. P., Johnson, P. V., McConkey, J. W., Ajello, J. M., & Kanik, I. (2008). Dissociative excitation of N_2O by electron impact. *Journal of Physics B: Atomic, Molecular and Optical Physics*, *41*(9), 095201. https://doi.org/10.1088/0953-4075/41/9/095201

Marinelli, W. J., Kessler, W. J., Green, B. D., & Blumberg, W. A. M. (1989). The radiative lifetime of N_2 (,v = 0-2). *The Journal of Chemical Physics*, *91*(2), 701–707. https://doi.org/10.1063/1.457175

Mason, N. J., & Newell, W. R. (1987). Electron-impact total excitation cross-section of the a $^1\Pi_g$ state of N_2. *Journal of Physics B: Atomic, Molecular and Optical Physics*, *20*, 3913–3921. https://doi.org/10.1088/0022-3700/20/15/035

McClintock, W. E., Schneider, N., Hosclaw, G. J., Clarke, J. T., Hoskins, A., Stewart, I., et al. (2015). The imaging ultraviolet spectrograph (IUVS) for the MAVEN mission. *Space Science Reviews*, *195*(1-4), 75–124. https://doi.org/10.1007/s11214-014-0098-7

Noren, C., Kanik, I., Ajello, J. M., McCartney, P., Makarov, O., McClintock, W. E., & Drake, V. (2001). Emission cross section of O I (135.6 nm) at 100 eV resulting from electon-impact dissociative excitation of O_2. *Geophysical Research Letters*, *28*(7), 1379–1382. https://doi.org/10.1029/2000GL012577

Strickland, D. J., Bishop, J. E., Evans, J. S., Majeed, T., Shen, P. M., Cox, R. J., et al. (1999). Atmospheric Ultraviolet Radiance Integrated Code (AURIC): Theory, software architecture, inputs, and selected results. *Journal of Quantitative Spectroscopy & Radiative Transfer*, *62*(6), 689–742. https://doi.org/10.1016/S0022-4073(98)00098-3

Strickland, D. J., Evans, J. S., & Paxton, L. J. (1995). Satellite remote sensing of thermospheric O/N_2 and solar EUV: 1. Theory. *Journal of Geophysical Research*, *100*(A7), 12,217–12,226. https://doi.org/10.1029/95JA00574

Tilford, S. G., & Benesch, W. M. (1976). Absorption oscillator strengths for the $a'^1\Sigma_u^- \rightarrow X^1\Sigma_g^+$ and $a'^1\Sigma_u^-$ and $w^1\Delta_u \rightarrow X^1\Sigma_g^+$ transitions of molecular nitrogen. *The Journal of Chemical Physics*, *64*, 3370–3374. https://doi.org/10.1063/1.432628

Wilkinson, P. G., & Mulliken, R. S. (1959). Forbidden band systems in nitrogen. II. The $a'^1\Sigma_u^- – X^1\Sigma_g^+$ system in absorption. *The Journal of Chemical Physics*, *31*, 674–679. https://doi.org/10.1063/1.1730445

Young, J. A., Malone, C. P., Johnson, P. V., Ajello, J. M., Liu, X., & Kanik, I. (2010). Lyman-Birge-Hopfield emissions from electron-impact excited N_2. *Journal of Physics B: Atomic, Molecular and Optical Physics*, *43*. https://doi.org/10.1088/0953-4075/43/13/135201